Synthesis, crystal structure, Hirshfeld surface analysis, DFT calculations, 3D energy frameworks studies of Schiff base derivative 2,2′-((*1Z,1′Z*)-(1,2-phenylene bis(azanylylidene)) bis(methanylylidene)) diphenol

Chandini KM [a,b], Fares Hezam Al-Ostoot [c,d], Eman E. Shehata [e], Nuha Y. Elamin [e], Hela Ferjani [e], Sridhar MA [a,*], Lokanath NK [a]

[a] *Department of Studies in Physics, University of Mysore, Manasagangotri, Mysuru 570 006, India*
[b] *Department of Physics, MMK and SDM Mahila Maha Vidyalaya, Mysuru 570004, India*
[c] *Department of Chemistry, Yuvaraja's College, University of Mysore, Mysuru 570 006, India*
[d] *Department of Biochemistry, Faculty of Education & Science, Al-Baydha University, Al-Baydha, Yemen*
[e] *Department of Chemistry, College of Science, IMSIU (Imam Mohammad Ibn Saud Islamic University), Riyadh 11623, Saudi Arabia*

ARTICLE INFO

ABSTRACT

The title compound 2,2′-((*1Z,1′Z*)-(1,2-phenylene bis(azanylylidene)) bis(methanylylidene)) diphenol was synthesized with a good yield. The crude product was recrystallized using ethanol and acetonitrile as solvent. Elemental analysis and spectroscopic analysis (NMR, LC-MS) were done to elucidate the structure. The compound was characterized by single crystal X-ray diffraction. The intermolecular interaction of the type and C−H···O between the molecules in a crystal was shown by Hirshfeld surface analysis. Intramolecular interactions of the type O−H···N was shown by atoms in molecule (AIM) theory calculations. The energy framework calculations revealed that the dispersion energy is dominant. The orbital energy gap between HOMO and LUMO was found to be 3.9678 eV. The charge distribution in the compound is visualised using molecular electrostatic potential surface.

© 2021 Published by Elsevier B.V.

Introduction

The emission of cations and anionic pollutants has increased the risks to human health and the environment due to uncontrolled agricultural and industrial activities [1]. The need for specific and sensitive identification of pollutant species (e.g., toxins and metal ions) is in high demand particularly in health and environmental applications [2, 3]. Structures from the Schiff base show incredible results for metal ion determination [4]. Schiff bases are generally compounds bearing imines or azomethines (-CH=N-) functional group, that work as ligands in different metal complexes. In several fields including analytical, biological and inorganic chemistry, Schiff bases represent an important class of organic compounds [5, 6]. In addition to detection, recognition, and identification of aldehydes or ketones, Schiff bases have a variety of applications including preparatory use, purification of carbonyl or amino molecules and protection of these groups throughout complex or sensitive reactions [7]. Apart from biological activities, they are used as pigments/dyes [8], catalysts [9], intermediate substances, corrosion inhibitors [10] and polymer stabilizers [11]. Recent reports indicated that Schiff bases can be used as extremely active and promising sensing materials [12–14].

Schiff bases are shown to be significant substances for the design of different biological, medicinal, pharmacological applications [15] (Fig. 1). Schiff bases of salicylaldehyde have demonstrated a framework that supports the development of new antiviral agents [16]. Schiff bases have gained prominence in the biomedical fields due to a wide variety of pharmacological activities such as anti-fungal [17], anti-bacterial, anthelmintic [18], anti-malarial [19], analgesic, anti-pyretic, anti-inflammatory [20], anti-convulsant [21], anti-cancer [22] and so forth. Formazans, 4-thiazolidinines, benzoxazines are prepared from Schiff bases synthons to have a variety of industrial and bioactive compounds [23, 24]. The researchers therefore, promoted the use of Schiff base derivatives in developing unique eco-friendly technologies [25]. In view of their broad spectrum of biological properties and as a part of our ongoing work [26–28], the synthesis and characterization

* Corresponding author at: Department of Studies in Physics, University of Mysore, Manasagangotri, Mysuru 570 006, India.
E-mail addresses: faresalostoot@gmail.com (F.H. Al-Ostoot), mas@physics.uni-mysore.ac.in (S. MA).
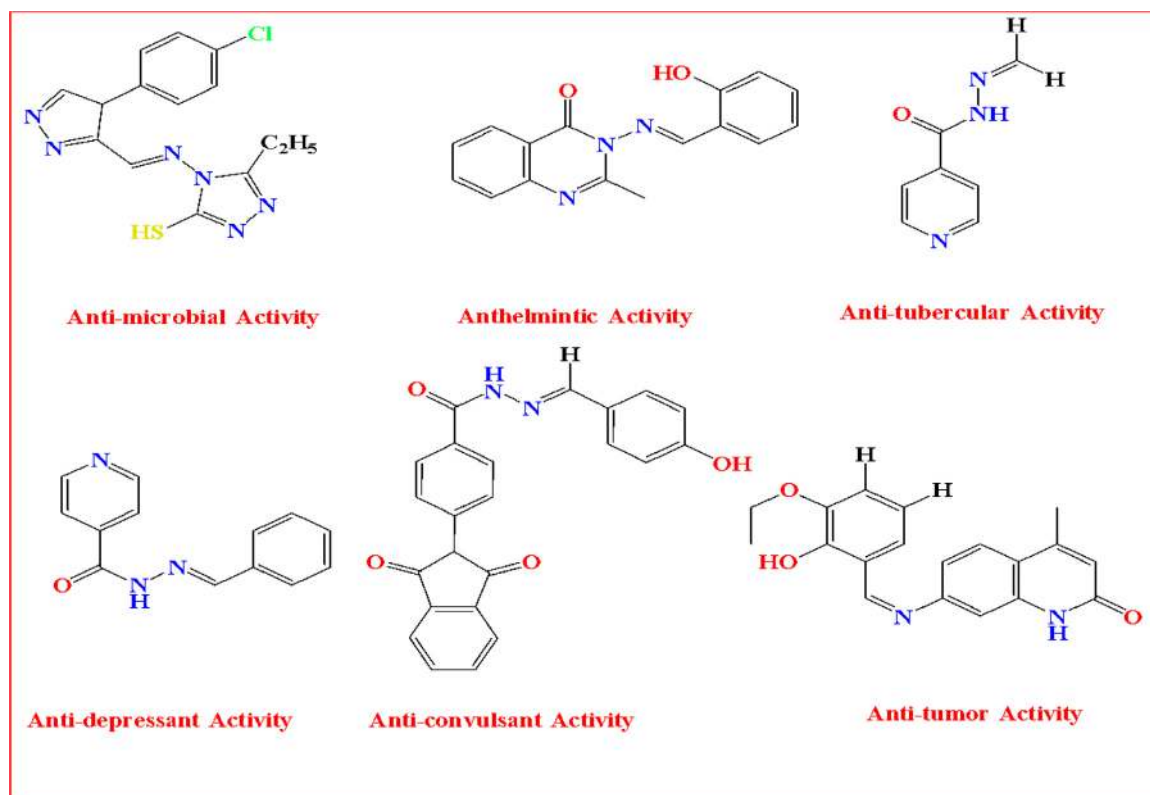
Fig. 1. Schiff base compounds shown different biological activities.

of title compound was carried out by single-crystal X-ray diffraction. The structure of the molecule was determined and characterized using different methods like NMR and elemental analysis. This study is also supplemented by Hirshfeld surface investigations and Density Functional Theory (DFT) calculations.

2. Experimental details

2.1. Materials and methods

Chemicals were purchased from Sigma Aldrich Chemical Company and TCI Chemical Pvt.Ltd, and used without further purification. Melting point was determined using the Chemi Line CL725 Micro Controller based melting point apparatus with a digital thermometer. The NMR (^{1}H ^{13}C) spectrum was recorded on a VNMRS-400 MHz Agilent-NMR spectrophotometer in DMSO, Mass spectrum was obtained with a VG70–70H spectrophotometer. Elemental analysis results are within ±0.5% of the calculated value.

2.2. Synthesis of 2,2′-((1Z,1′Z)-(1,2-phenylene bis(azanylylidene)) bis(methanylylidene)) diphenol

The compound 2,2′-((1Z,1′Z)-(1,2-phenylene bis(azanylylidene)) bis(methanylylidene)) diphenol (**3**) was accomplished by a synthetic procedure as shown in Scheme 1. A solution of 2-hydroxybezaldehyde (**1**, 5 ml) was mixed with 60 ml of ethanolic solution of o-phenylene diamine (**2**, 2 mmol, 0.223 gm) in molar ratio 1:2. The reaction mixture was stirred and refluxed for 30 min and monitored by TLC using mobile phase system [hexane: ethyl acetate (3:1)]. The yellow precipitate formed was then cooled to room temperature, filtered, washed several times with mixture of water and ethanol. The precipitate was dried to obtain a crude product, which on recrystallization with system of ethanol:acetonitrile (6:2) formed the compound as colourless crystals. The melting point (M.P) of the compound was found to be 165 °C.

2.3. Spectral data

2,2′-((1Z,1′Z)-(1,2-phenylene bis(azanylylidene)) bis(methanylylidene)) diphenol (3). Yield 80%; M.P. 165–167 °C; ^{1}HNMR (400 MHz, DMSO–d$_6$) δ (ppm): 6.90–7.39 (m, 6H, Ar-H), 8.63 (s, 1H, HC=N), 13.03 (s, 1H, OH) (Fig. 2); ^{13}C NMR (400 MHz, DMSO) δ: 117.55 (1C, Ar-C), 118.95 (1C, Ar-C), 119.20 (1C, Ar-C), 119.73 (1C, Ar-C), 127.66 (1C, Ar-C), 132.31 (1C, Ar-C) 142.56 (1C, Ar-C), 161.33 (1C, $C = N$), 163.72 (1C, Ar-C-OH) (Fig S1); LC-MS m/z: 316 [$M+$]. Anal.Calcd.for C$_{20}$H$_{16}$N$_2$O$_2$(316): C, 75.93; H, 5.11; N, 8.85. Found: C, 75.90; H, 5.08; N, 8.84%.

2.4. Data collection and reduction

A single crystal of about 0.18χ0.19χ0.20 mm was chosen for X-ray diffraction data collection. X-ray intensity data were collected on a Rigaku X-ray diffractometer equipped with radiation Mo$K\alpha$ of wavelength 0.71073 Å. The data were collected at 293 K. Crystal structure was solved by direct methods using *SHELXS-97* program [29]. A total of 2000 phase sets were refined, with the correct phase set having combined figure of merit CFOM=0.0661. An E-map drawn with the correct phase set revealed all the non-hydrogen atoms.

The structure was refined using *SHELXL-97* [29] against F^2 by full matrix least-squares method. All the non-hydrogen atoms were refined anisotropically. The hydrogen atoms were placed at chemically acceptable positions, and were allowed to ride on their parent atoms. A total of 2926 parameters were refined with 298 unique reflections which converged the R value to 0.0780. The final weight factor wR_2 was 0.1808, and goodness-of-fit S was 1.099. The geometrical calculations were performed using *PLATON* [30]. The *OR-*
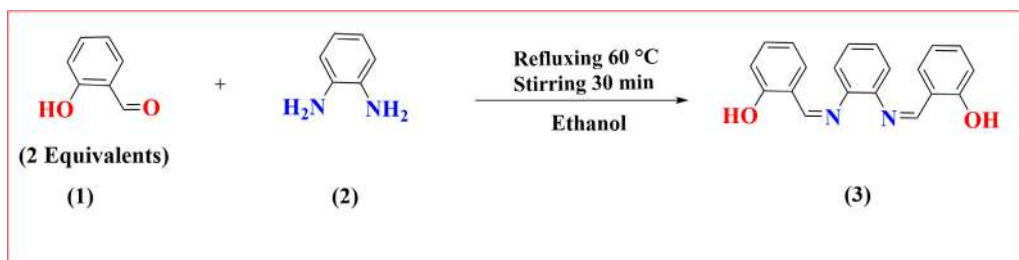
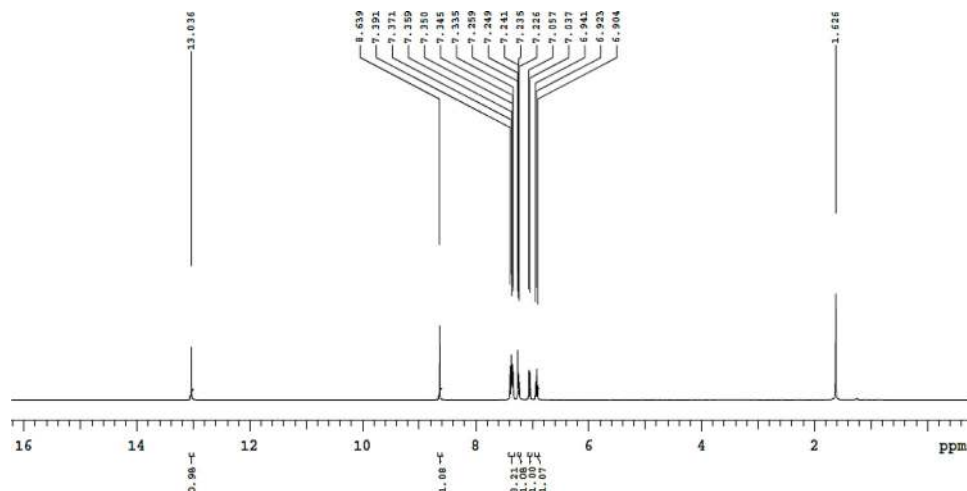**Scheme 1.** Schematic representation of the synthesis of the title compound (3).

Fig. 2. ^{1}HNMR spectrum of title compound (3).

TEP and molecular packing diagrams were generated using *MERCURY* software [31].

3. Results and discussion

3.1. Synthesis

The title compound (**3**) was accomplished by a synthetic procedure as shown in Scheme 1. Initially a solution of 2-hydroxybezaldehyde (**1**), was mixed with ethanolic solution of o-phenylene diamine (**2**). The reaction mixture was then stirred and refluxed for 30 min and monitored by TLC. Finally, the precipitate of compound (**3**) was formed and then cooled to room temperature, filtered, washed several times with mixture of water and ethanol. The structure of the newly synthesised compound was assigned on the basis NMR, LC-MS spectroscopic data and also by C, H, and N analysis. The ^{1}H NMR spectrum of compound (**3**) has shown the disappearance of protons of both NH_2 groups of compound (**2**), and the appearance of two protons at δ 8.63 corresponding for the imine group -CH=N. Besides, the mass spectrum gave significant stable $M +$ peak at m/z 316, which clearly affirmed the formation of compound (**3**).

3.2. X-ray diffraction

The title compound C$_{20}$H$_{16}$N$_2$O$_2$ is crystallized in the monoclinic crystal system with space group $P\,2_1/c$. The unit cell parameters are $a = 6.002(8)$ Å, $b = 16.55(2)$ Å, and $c = 16.33(2)$ Å and $\beta = 91.60°$ The crystal data and structure refinement details are listed in Table 1. The *ORTEP* of the molecule with thermal ellipsoids drawn at 50% probability is shown in Fig. 3. The bond lengths, bond angles and torsion angles are listed in Tables 2, 3, and 4 respectively.
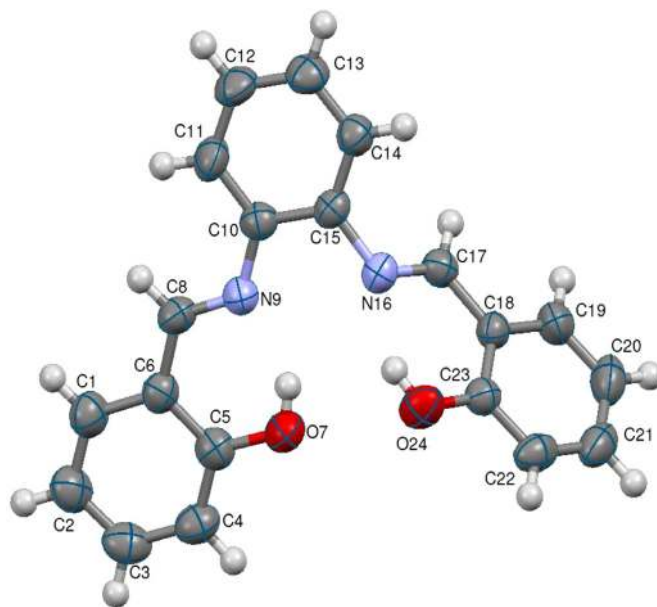

Fig. 3. ORTEP of the molecule with thermal ellipsoids drawn at 50% probability.

The crystal structure comprises three six membered rings. The phenyl rings are connected to benzene ring by schiff bases (-$C = N$-). The carbon atoms in the phenyl rings (C1-C2-C3-C4-C5-C6) and (C18-C19-C20-C21-C22-C23) are sp^2 hybridized and has nearly planar trigonal geometry evident from bond angle values C2-C3-C4 = 121.3(4)°, C3-C4-C5 = 120.6(4)°C18-C19-C20 = 120.7(4)°. The planarity of the rings can be understood by torsion angle val-

Table 1
Crystal data and structure refinement details.

Parameter	Value
CCDC number	2060415
Empirical formula	$C_{20} H_{16} N_2 O_2$
Formula weight	316.35
Temperature	293 K
Wavelength	0.71073 Å
Crystal system	Monoclinic
Space group	$P 2_1 /c$
Cell Dimensions	$a = 6.002 (8)$Å$b = 16.55 (2)$ Å$c = 16.33 (2)$ Å$\beta = 91.60$ °
Volume	1622 (4) Å^3
Z	4
Density(calculated)	1.296 Mg m^{-3}
Absorption coefficient	0.085 mm^{-1}
F_{000}	664
Crystal size	0.18 mm $\times$ 0.19 mm $\times$ 0.20 mm
θ range for data collection	3.51° to 27.57°
Index ranges	$-4 \leq h \leq 7 - 20 \leq k \leq 20 - 10 \leq l \leq 20$
Reflections collected	6042
Independent reflections	2926 [$R_{int} = 0.066$]
Absorption correction	Multi-scan
Refinement method	Full matrix least-squares on F^2
Data / restraints/ parameters	2926 / 0 / 218
Goodness-of-fit on F^2	1.099
Final [$I > 2\sigma(I)$]	$R1 = 0.0780$, $wR2 = 0.1808$
R indices (all data)	$R1 = 0.1375$, $wR2 = 0.2152$
Extinction coefficient	0.003(3)
Largest diff. peak and hole	0.153 and -0.217 e Å^{-3}

Table 2
Bond lengths.

Atoms	Length (Å) XRD	DFT	Atoms	Length (Å) XRD	DFT
O7-C5	1.347(5)	1.3408	C10-C15	1.404(5)	1.4198
O24-C23	1.355(5)	1.3407	C10-C11	1.398(5)	1.4033
N9-C8	1.273(5)	1.2930	C11-C12	1.380(6)	1.3907
N16-C17	1.275(5)	1.2930	C13-C14	1.380(5)	1.3907
N16-C15	1.420(5)	1.4129	C14-C15	1.392(5)	1.4033
C1-C6	1.404(5)	1.4092	C17-C18	1.456(5)	1.4491
C1-C2	1.385(6)	1.3856	C18-C23	1.400(5)	1.4237
C2-C3	1.389(7)	1.4037	C18-C19	1.389(5)	1.4093
C3-C4	1.369(7)	1.3888	C19-C20	1.382(6)	1.3855
C4-C5	1.397(6)	1.4033	C20-C21	1.390(7)	1.4038
C5-C6	1.406(5)	1.4237	C21-C22	1.376(6)	1.3887
C6-C8	1.446(5)	1.4490	C22-C23	1.385(5)	1.4033

Table 3
Bond angles.

Atoms	Angle (°) XRD	DFT	Atoms	Angle (°) XRD	DFT
C8-N9-C10	123.7(3)	121.19	C11-C12-C13	120.9(4)	199.67
C15-N16-C17	119.3(3)	121.19	C12-C13-C14	119.5(4)	119.67
C2-C1-C6	122.3(3)	121.27	C13-C14-C15	120.8(3)	121.47
C1-C2-C3	118.2(4)	119.09	C10-C15-C14	120.0(3)	118.82
C2-C3-C4	121.3(4)	121.11	N16-C15-C14	121.3(3)	116.87
C3-C4-C5	120.6(4)	120.16	N16-C15-C10	118.6(3)	124.31
O7-C5-C6	121.1(3)	121.88	N16-C17-C18	121.8(3)	122.12
C4-C5-C6	119.8(3)	199.37	C19-C18-C23	119.4(3)	119.00
O7-C5-C4	119.1(3)	188.75	C17-C18-C19	119.0(3)	119.81
C5-C6-C8	121.0(3)	121.19	C17-C18-C23	121.6(3)	121.19
C1-C6-C5	117.8(3)	119.00	C18-C19-C20	120.7(4)	121.26
C1-C6-C8	121.2(3)	119.82	C19-C20-C21	119.3(4)	119.10
N9-C8-C6	122.1(3)	122.13	C20-C21-C22	120.8(4)	121.11
N9-C10-C15	116.4(3)	124.31	C21-C22-C23	120.0(4)	120.17
C11-C10-C15	118.0(3)	118.81	C18-C23-C22	119.8(3)	119.36
N9-C10-C11	125.6(3)	116.87	O24-C23-C18	121.9(3)	121.88
C10-C11-C12	120.9(4)	121.47	O24-C23-C22	118.3(3)	118.76

ues C2-C3-C4-C5 = 0.6(7)°, C3-C4-C5-C6 = 0.3(6)°, C19-C20-C21-C22 = 1.0(6)°, C20-C21-C22-C23 = −0.1(6)°.

The benzene ring (C10-C11-C12-C13-C14-C15) is also sp^2 hybridized and has trigonal planar geometry. The bond angles C10-C11-C12 = 120.9(4)°, C11-C12-C13 = 120.9(4)° and torsion angle values are C10-C11-C12-C13 = 0.3(6)°, C12-C13-C14-C15 = 0.7(6)°.

The crystal structure shows intramolecular interactions of the type O7-H7···N9, O24-H24···N16 and intermolecular hydrogen bond of the type C17-H17···O7 (Table 5). The structure has C−H···π and π-π interactions. The interaction details are given in Tables 6 and 7 respectively. The molecular packing viewed down *b* axis is shown in Fig. 4.

Table 8
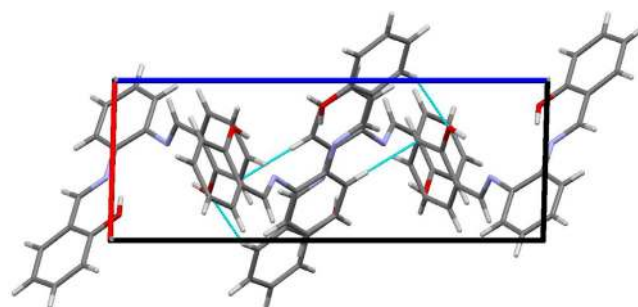
Fig. 4. Packing the molecules viewed down the *b*-axis.

3.3. Hirshfeld surface analysis

Hirshfeld surface analysis is a valuable tool to elucidate the intermolecular interactions in a crystal structure. *CrystalExplorer 17.5* [32] software was used to generate the Hirshfeld surface mapped over d_{norm} (Fig. 5). The normalized contact distance d_{norm} is defined as

$$d_{norm} = \frac{d_i - r_i^{vdw}}{r_i^{vdw}} + \frac{d_e - r_e^{vdw}}{r_e^{vdw}},$$

Table 4
Torsion angles.

Atoms	Angle (°)		Atoms	Angle (°)	
	XRD	DFT		XRD	DFT
C10-N9-C8-C6	179.8(3)	179.85	N9-C10-C15-C14	175.7(3)	−177.19
C8-N9-C10-C11	−1.6(6	−128.90	C11-C10-C15-N16	175.1(3)	−177.19
C8-N9-C10-C15	−178.1(3	52.2	C11-C10-C15-C14	1.1(5)	3.75
C17-N16-C15-C10	131.7(3	52.2	C10-C11-C12-C13	0.3(6)	0.5
C15-N16-C17-C18	176.3(3	179.85	C11-C12-C13-C14	−1.1(6)	0.64
C6-C1-C2-C3	−0.7(6)	−0.04	C12-C13-C14-C15	0.7(6)	0.50
C2-C1-C6-C5	1.0(5)	0.09	C13-C14-C15-N16	−175.8(3)	178.16
C2-C1-C6-C8	−176.9(4)	179.98	C13-C14-C15-C10	0.4(5)	−2.71
C1-C2-C3-C4	−0.1(7)	−0.02	N16-C17-C18-C19	175.8(3)	179.77
C2-C3-C4-C5	0.6(7)	0.04	N16-C17-C18-C23	−4.6(5)	−0.35
C3-C4-C5-O7	179.7(4)	−179.97	C17-C18-C19-C20	178.1(3)	179.98
C3-C4-C5-C6	−0.3(6)	0.01	C23-C18-C19C20	−1.5(5)	0.10
O7-C5-C6-C1	179.5(3)	179.91	C17-C18-C23-O24	1.9(5)	0.02
O7-C5-C6-C8	−2.5(5)	0.02	C17-C18-C23-C22	−177.2(3)	−179.96
C4-C5-C6-C1	−0.5(5)	−0.08	C19-C18-C23-O24	−178.5(3)	179.90
C4-C5-C6-C8	177.5(3)	−179.96	C19-C18-C23-C22	2.4(5	−0.08
C1-C6-C8-N9	175.5(3)	179.77	C18-C19-C20-C21	−0.2(6)	−0.05
C5-C6-C8-N9	−2.4(5)	−0.34	C19-C20-C21-C22	1.0(6)	−0.02
N9-C10-C11-C12	−175.7(4)	178.16	C20-C21-C22-C23	−0.1(6)	0.04
C15-C10-C11-C12	0.8(6)	−2.71	C21-C22-C23-O24	179.3(3)	−179.97
N9-C10-C15-N16	−8.0(5)	1.88	C21-C22-C23-C18	−1.6(5)	0.01

Table 5
Hydrogen bond geometry.

Atoms	D - H (Å)	H···A (Å)	D - A (Å)	D - H···A (°)
O7-H7···N9[a]	0.82	1.85	2.579(3)	148
O24-H24···N16[a]	0.82	1.89	2.618(3)	147
C17-H17···O7[i]	0.93	2.46	3.315(4)	152

i: 1 + x, y, z.
a: intramolecular interactions.
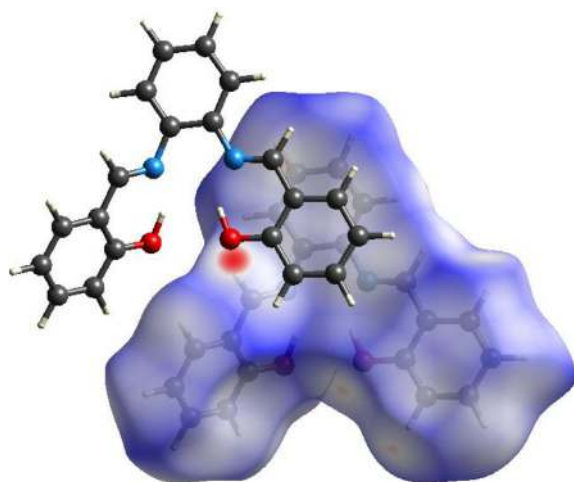
Fig. 5. Hirshfeld surface of the molecule mapped for d_{norm}.

where r_i and r_e are the van der Waals (vdw) radii of the appropriate atom internal and external to the surface respectively; d_e and d_i are the distance from a point on the surface to the nearest

nucleus outside and inside the surface respectively [33]. The red highlighted spots and blue regions on the d_{norm} surface are from the short contacts and longer contacts less than the sum of van der Waals radii respectively.

Hirshfeld surface mapped for shape index and curvedness is shown in Fig. 6. The planar stacking arrangements and contact with the adjacent molecule are visualized from the shape index and the curvedness mapping. The complementary hollows which is red in color and blue bumps shows the molecular surfaces touching each other [34]

The percentage contribution of intermolecular interactions to the total surface area of the molecule is visualized by two dimensional fingerprint plots [35]. The fingerprint plots of d_i and d_e are shown in Fig. 7. The significant contributions are from C–H, H–H, and O–H contacts. The blue - green regions on the fingerprint plots indicate the π-π interactions.

3.4. Energy frameworks

The interaction energies between the molecular pairs in a crystal structure is visualized by energy frameworks. The energy frameworks were generated for molecules within 3.8 Å radius from the central molecule using *CrystalExplorer 17.5* [32] software with the functional basis set B3LYP/6 −31 G(d, p) [36]. The molecular pairs involved in the interaction energy calculations are shown in figure S2. The energy frameworks generated for Coulomb, dispersion and total energy are represented by different color cylinders joining the center of mass of the molecules with cutoff energy 5 kJ mol^{-1} (Fig. 8).

The elecrostatic (−51.89 kJ mol^{-1}), polarization (−10.656 kJ mol^{-1}), dispersion (−187.87 kJ mol^{-1}), and repulsive (83.61 kJ mol^{-1}) energy terms gives the total interaction energy (−166.7 kJ mol^{-1}). Dispersion energy is dominant over electrostatic and polar-

Table 6
C–H···π interaction involved in the molecular structure.

C···H	CgJ	H···Cg (Å)	H⊥ (Å)	γ (°)	C–H···Cg (°)	C···Cg (Å)	C–H···π (°)
C3 – H3	Cg3[ii]	2.84	2.83	4.84	140	3.603(7)	48
C21 –H21	Cg2 [iii]	2.89	−2.86	9.18	163	3.796(7)	73

ii: − x, 1 − y, 2 − z.   iii: 1 − x, 1/2 + y, 3/2 − z
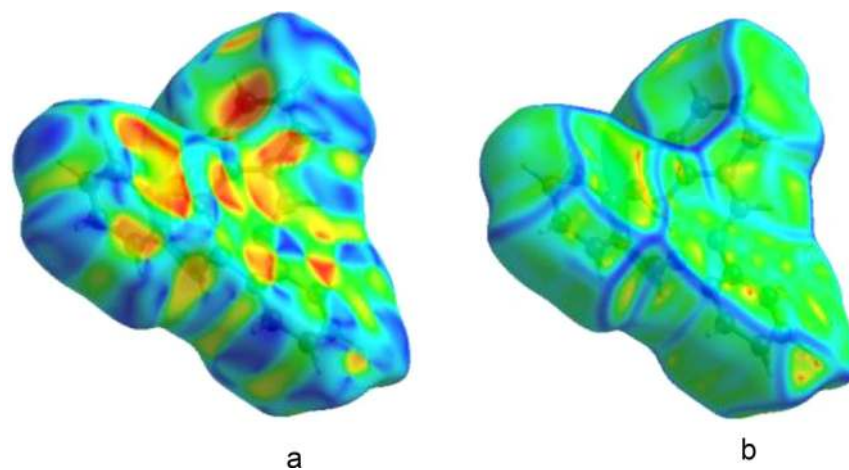Cg2: C10-C11-C12-C13-C14-C15   Cg3: C18-C19-C20-C21-C22-C23

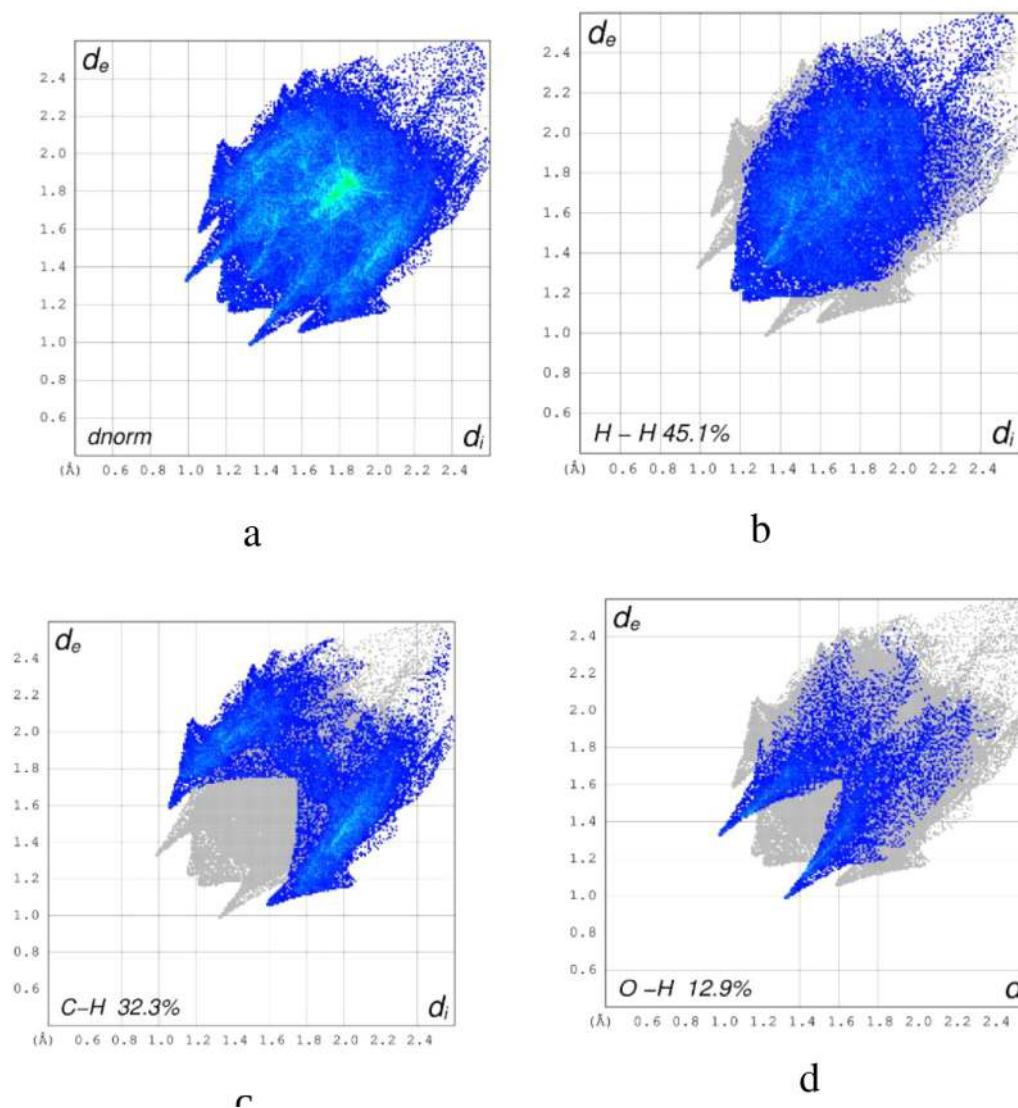**Fig. 6.** Hirshfeld surface of the molecule mapped for shape index (*a*) and curvedness (*b*).

Fig. 7. Fingerprint plots of the compound showing percentage contributions for the total Hirshfeld surface.

Table 7
π -π interaction involved in the molecular structure.

CgI	CgJ	CgI-CgJ	α (°)	β(°)	γ(°)	CgI⊥ (Å)	CgJ⊥ (Å)	Slippage (Å)
Cg1	Cg2^{iv}	3.769(5)	3.30(19)	23.7	22.1	3.4921(16)	−3.4511(16)	1.515
Cg1	Cg3^{v}	4.900(7)	56.84(18)	8.3	63.6	2.1823(16)	4.8495(16)	–
Cg2	Cg1^{vi}	3.769(5)	3.30(19)	22.1	23.7	−3.4510(16)	3.4919(16)	1.418
Cg2	Cg3^{vii}	5.150(7)	83.42(18)	10.2	88.4	−0.1441(16)	−5.0677(16)	–
Cg3	Cg1^{viii}	4.849(7)	56.84(18)	19.7	70.9	1.5899(16)	4.5636(16)	–
Cg3	Cg2^{ix}	5.132(7)	83.42(18)	11.9	85.4	0.4117(16)	−5.0207(16)	–

iv: −1 + x, y, z

v: 1 − x, 1 − y, 2 − z

vi: − x, 1- y, 2 − z

Cg1:C1-C2-C3-C4-C5-C6

Cg3: C18-C19-C20-C21-C22-C23

vii: 1 + x, y,

viii: 1 + x, 1/2 + y, 3/2 − z

ix: 1 − x, −1/2 + y, 3/ 2 − z

Cg2:C10-C11-C12-C13-C14-C15
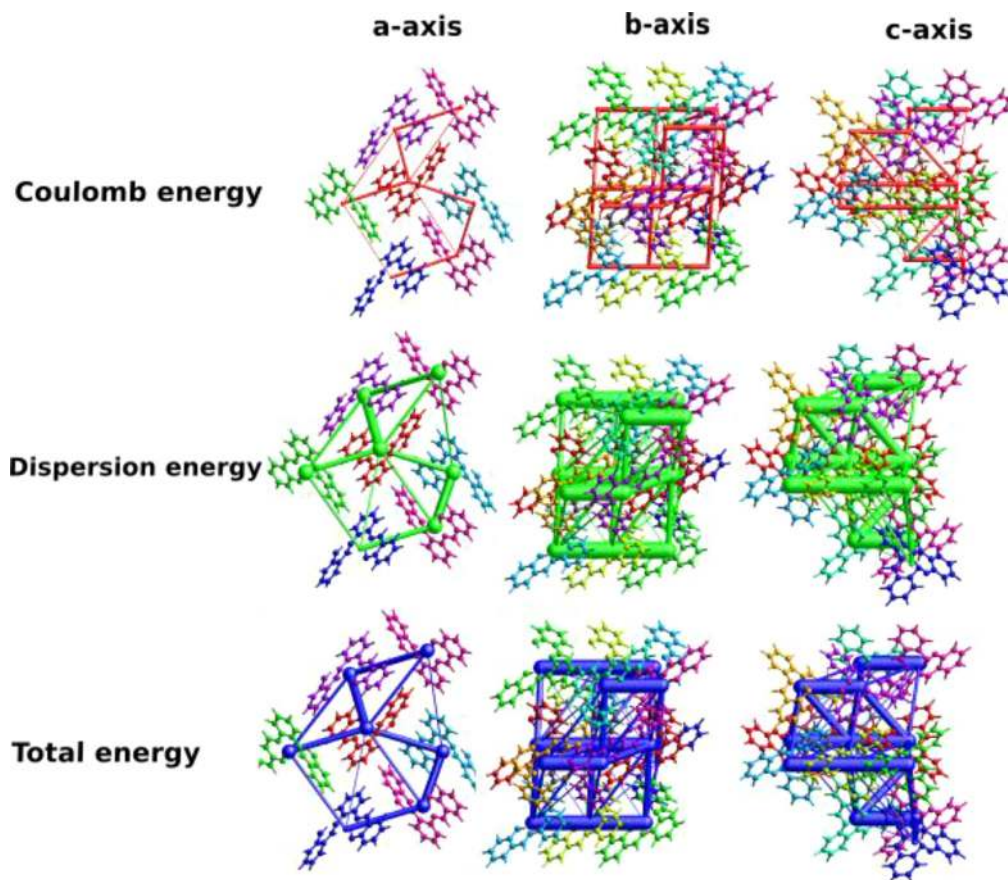
Fig. 8. Graphical representation of the interaction energies Coulomb energy, Dispersion energy and Total energy along *a,b, c* axes.

Table 8
Percentage contributions to the total Hirshfeld surface area from various intermolecular contacts .

Intermolecular Contacts	Contribution (%)
H – H	45.1
C – H	32.3
O – H	12.19
C – C	5.5
N – H	2.3
C – N	1.9

ization energies. The lattice energy of the molecule is −137.85 kJ mol^{-1}. The molecular interaction energies are calculated and listed in table 9 with scale factor k_ele = 1.057, k_pol =0.740, k_disp=0.871, k_rep =0.618.

3.5. Density functional theory

3.5.1. Frontier molecular orbitals

Density functional theory (DFT) calculations were performed using *Gaussian 09* [37] package with B3LYP hybrid functional and 6–31 G (d, p) basis set in gas phase. Molecular orbitals were visualized in *GaussView* [38]. The bond length, bond angle, torsion angles calculated from DFT calculations are in good agreement with results from single crystal Xray diffraction. Highest occupied molecular orbital (HOMO) and lowest unoccupied molecular orbital (LUMO) of the compound are shown in Fig. 9. The energy gap between LUMO and HOMO is 3.9678 eV.

The global parameters such as ionization potential, electron affinity, chemical potential, chemical hardness, electronegativity, electrophilicity, global softness are listed in Table 10.

The total density of states (TDOS) are created by convoluting the molecular orbital information with Gaussian curves of unit

Table 9

Interaction energies of the molecular pairs involved in energy calculation in kJ/mol. R is the distance betweeen molecular centroids in Å and N is the number of molecular pairs involved.

	N	Symop	R	Electron Density	E_ele	E_pol	E_dis	E_rep	E_tot
	2	x, y, z	6.00	B3LYP/6-31G(d,p)	-17.8	-4.7	-70.6	47.9	-54.1
	1	-x, -y, -z	7.91	B3LYP/6-31G(d,p)	-10.5	-3.6	-41.6	30.8	-31.0
	2	x, -y+1/2, z+1/2	8.54	B3LYP/6-31G(d,p)	-11.1	-2.6	-23.9	18.7	-22.9
	2	x, -y+1/2, z+1/2	10.30	B3LYP/6-31G(d,p)	-0.2	-0.2	-3.7	0.7	-3.1
	2	-x, y+1/2, -z+1/2	10.37	B3LYP/6-31G(d,p)	-3.5	-0.4	-13.8	6.7	-11.9
	2	x, -y+1/2, z+1/2	10.57	B3LYP/6-31G(d,p)	-0.7	-0.7	-15.7	5.6	-11.4
	1	-x, -y, -z	13.01	B3LYP/6-31G(d,p)	-0.7	-0.4	-9.2	6.7	-4.9
	1	-x, -y, -z	6.21	B3LYP/6-31G(d,p)	-3.2	-1.5	-28.5	12.2	-21.8
	2	-x, y+1/2, -z+1/2	12.58	B3LYP/6-31G(d,p)	-1.4	-0.3	-8.7	6.0	-5.6
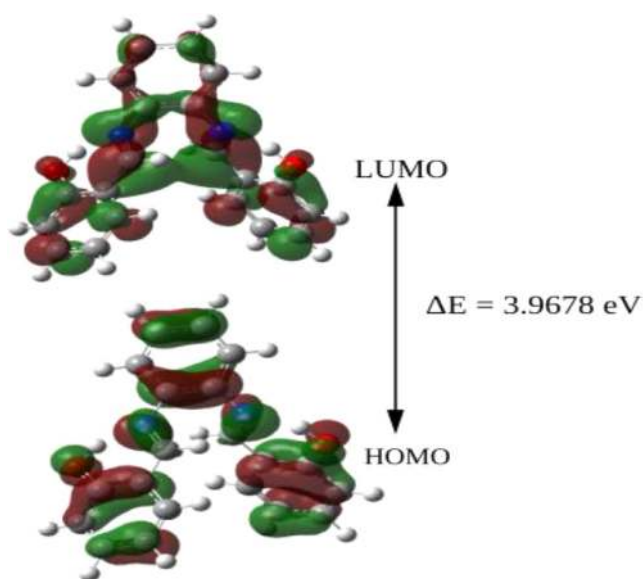
Fig. 9. HOMO and LUMO of the title compound.

$\Delta E = 3.9678$ eV

Fig. 10. Molecular Electrostatic Potential Surface.

Table 10

Calculated energy values of HOMO, LUMO and electronic properties of the title compound.

Parameter	Value
ELUMO	−1.8161 eV
EHOMO	−5.7839 eV
ΔE	3.9678 eV
Ionization potential (I)	5.7839 eV
Electron affinity (A)	1.8161 eV
Chemical potential μ	−3.8 eV
Chemical Hardness η	1.9839 eV
Electronegativity χ	3.8 eV
Electrophilicity ω	3.64 eV
Global softness σ	0.50 eV^{-1}
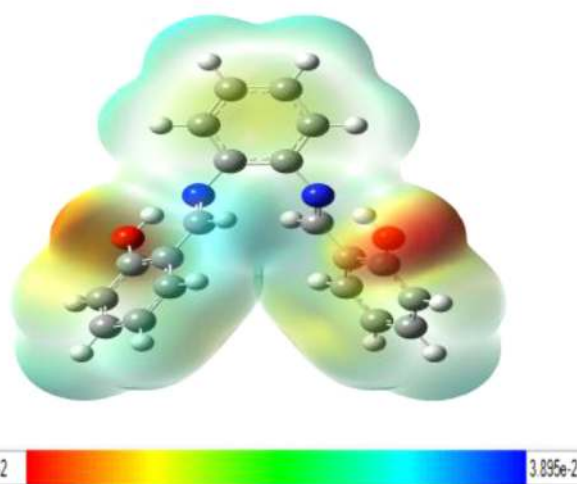
height and full width at half maximum (FWHM) [39] by using the Gauss-Sum 2.2 program [40]. The plot of TDOS gives the graphical representation of compositions of the molecular orbital's and their contributions to chemical bonding figure S3.

3.5.2. Molecular electrostatic potential

The electropositive and electronegative regions of the molecule are visualized as molecular electrostatic potential surface. The map gives a spectral display of increasing potential value from red to blue (Fig. 10). The potential value ranges from −3.895e-2 a.u. (red) to +3.895e-2 a.u. (blue) for the molecule under discussion. The red and blue regions on the molecular electrostatic potential surface indicate electrophilic and nucleophilic regions respectively [41].

Mulliken atomic charges with hydrogen atoms summed into heavy atoms were calculated using B3LYP / 6 −31 G (d, p) basis set and plotted (Fig. 11). The nitrogen atoms N9 and N16 are more
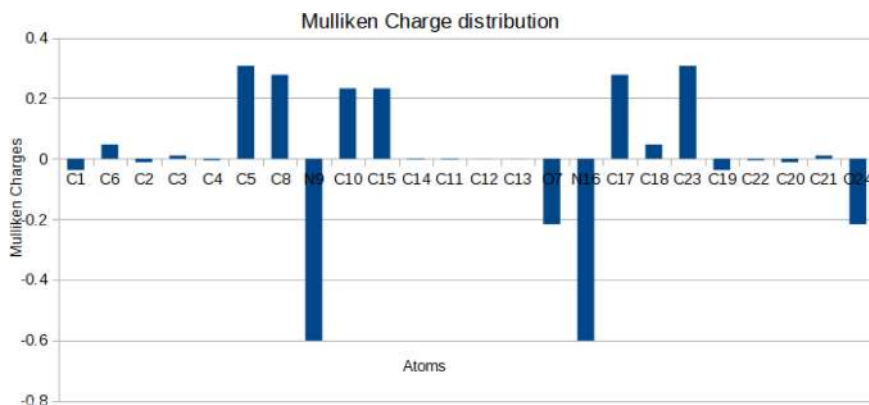
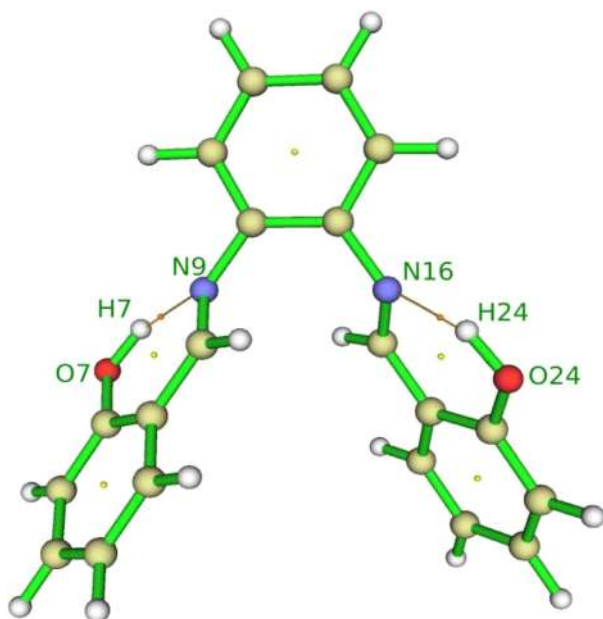**Fig. 11.** Mulliken charge distribution of the title compound.

Fig. 12. Intramolecular interactions of the title compound from AIM theory.

Fig. 13. RDG plot showing non covalent bond interactions in the title compound.

electronegative and carbon atoms C5, C17, C8 are more electropositive [42].

3.5.3. Atoms in molecule (AIM) theory

The topological analysis of atoms in molecule (AIM) gives the information about the presence of strong and weak hydrogen bonds. AIM analysis is used to find the intramolecular hydrogen bond interactions through bond critical paths. AIM analysis was performed using *Multiwfn 3.7* [43] program to examine the non-covalent interactions of the title molecule. Neighboring atoms which are chemically bonded or those atoms that have weak interactions appear in the Bond Critical Paths (BCP). The topology analysis of AIM was done to search all the bond critical points. The paths generated are shown in Fig. 12. The presence of BCP validates the O7-H7···N9 and O24-H24···N16 intramolecular interactions which are also obtained from XRD analysis.

3.5.4. Reduced density gradient (RDG) analysis

RDG analysis is used to explore the non-covalent bond interactions present in the molecule [44]. The non-covalent bond interactions are visualized by plotting RDG vs electron density (ρ). The strong attractions, van der Waals interactions, and strong repulsions are distinguished in Fig. 13. The calculations were performed
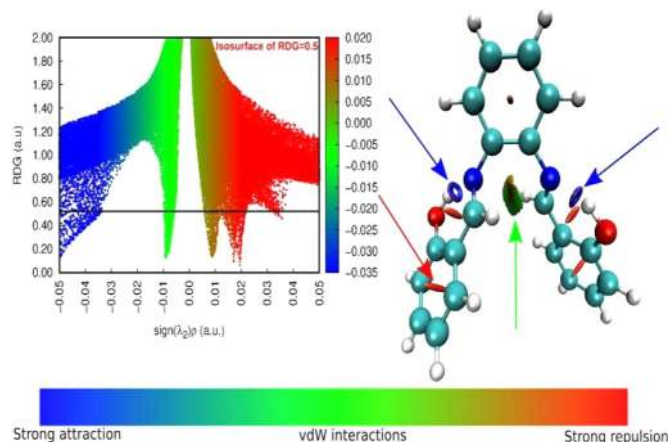
using *Multiwfn* software and visualized in *VMD (Visual Molecular Dynamics)* software [45]. From the Fig. 13 one can observe that the title molecule displayed strong attractions around the nitrogen atoms, strong repulsions in the six membered rings, and van der Waals interactions occured between two nitrogen atoms.

Multiple spikes are found in the scatter density plot (Fig. 13). These spikes are divided in to three regions according to the values of sign $(\lambda_2)\rho$. These regions are identified by different colours. The spikes that lie in the low density region indicates the H-bond interaction present in the molecule. Blue colored isosurfaces which lie between H7 and N9, H24 and N16 atoms respectively signify the characteristics of strong H-bond interaction. Due to the high electronegative nature of oxygen and electropositive nature of nitrogen, a strong interaction which is attractive in nature, is observed in the molecule. In Fig. 13, green colored isosurface lies between the two nitrogen atoms and signifies the presence of weak H-bond interaction. The red colored isosurfaces indicate the steric effect present in the ring due to strong repulsions.

4. Conclusion

The title compound exhibits short intermolecular interactions C17-H17···O7 and intramolecular interactions O7-H7···N9 and O24-H24···N16. The packing of the molecules is reinforced by C−H···π and π-π interactions. From Hirshfeld surface analysis fingerprint plot shows that the major contribution for total Hirshfeld surface area is from H−H contacts (45.1%). Interaction energy calculations reveal that dispersion energy is dominant. Density function theory calculations show that the energy gap between HOMO and LUMO

is 3.9678 eV. MEP map and Mulliken charge analyses show reactive sites present in the molecule. The intramolecular interactions are validated using AIM calculations. RDG analysis reveals the presence of weak interactions, strong attractions, and strong repulsions in the title compound.

Declaration of Competing Interest

The authors declare that they have no known competing financial interests or personal relationships that could have appeared to influence the work reported in this paper. This manuscript has not been submitted to, nor is under review at, another journal or other publishing venue. The authors have no affiliation with any organization with a direct or indirect financial interest in the subject matter discussed in the manuscript.

CRediT authorship contribution statement

Chandini KM: Formal analysis, Writing - review & editing. **Fares Hezam Al-Ostoot:** Formal analysis, Writing - original draft. **Eman E. Shehata:** Investigation, Methodology. **Nuha Y. Elamin:** Investigation, Methodology. **Hela Ferjani:** Investigation, Methodology. **Sridhar MA:** Project administration, Supervision, Validation. **Lokanath NK:** Data curation.

Acknowledgment

Supplementary materials

Supplementary material associated with this article can be found, in the online version, at doi:10.1016/j.molstruc.2021.130910.

References

[1] T.A. Laniyan, A.J. Adewumi, Helalth risk assesment of heavy metal pollution in groundwater around an exposed dumpsite in Southwestern Nigeria, J. Health Pollut. 9 (24) (2019) 191210, doi:10.5696/2156-9614-9.24.191210.

[2] A.L. Berhanu, I.MohiuddinM. Gaurav, A.K. Malik, J.S. Aulakh, V. Kumar, K.H. Kim., A review of the applications of Schiff bases as optical chemical sensors, TrAC. 1-116 (2019) 74–91, doi:10.1016/j.trac.2019.04.025.

[3] M. Orojloo, S. Amani, Colorimetric detection of pollution trivalent cations and HSO_4^- in aqueous media using a new Schiff-base probe: an experimental and DFT studies, Polycycl. Aromat. Compd. 27 (2019) 1–4, doi:10.1080/10406638.2019.1567561.

[4] A.M. Abu-Dief, I.M.A. Mohamed, A review on versatile applications of transitionmetal complexes incorporating Schiff bases, Beni-Suef Univ. J. Appl. Sci. (2015), doi:10.1016/j.bjbas.2015.05.004.

[5] M.N. Uddin, Z.A. Siddique, N. Mase, M. Uzzaman, W. Shumi., Oxatitanium(IV) complexes of some bis-unsymmetric Schiff bases: synthesis, structural elucidation and biomedical applications, Appl. Organomet. Chem. 33 (6) (2019) e4876, doi:10.1002/aoc.4876.

[6] P. Ghosh, S.K. Dey, M.H. Ara, K. Karim, A.B.M. Nazmul Islam, A review on synthesis and versatile applications of some selected Schiff bases with their complexes, Egypt. J. Chem. (2020) Apr 1 63(Special Issue (Part 2) Innovation in Chemistry) 5-6, doi:10.21608/ejchem.2019.13741.1852.

[7] A. Manimaran, R. Prabhakaran, T. Deepa, K. Natarajan, C. Jayabalakrishnan, Synthesis, spectral characterization, electrochemistry and catalytic activities of Cu(II) complexes of bifunctional tridentate Schiff bases containing O-N-O donorws, Appl. Organamet. Chem. 22 (7) (2008) 353–358, doi:10.1002/aoc.1400.

[8] M. Abdel-Shakour, W.A. El-Said, I.M. Abdellah, R. Su, A. El-Shafei, Low-cost Schiff bases chromophores as efficient co-sensitizers for MH-13 in dye-sensitized solar cells, J. Mater. Sci. 30 (5) (2019) 5081–5091, doi:10.1007/s10854-019-00806-2.

[9] M. Karman, G. Romanowski, Cis-dioxidomolybdenum(VI) complexes with chiral tetradentate Schiff bases:synthesis, spectroscpoic characterization and catalytic activity in sulfoxidation and epoxidation, Inorganica Chim. Acta. 511 (2020) 119832 1, doi:10.1016/j.ica.2020.119832.

[10] P. Shetty, Schiff bases: an overview of their corrosion inhibition activity in acid media against mild steel, Chem Eng Commun 2 207 (7) (2020) 985–1029, doi:10.1080/00986445.2019.1630387.

[11] L.H. Abdel-Rahman, A.M. Abu-Dief, M.S. Adam, S.K. Hamdan, ome new nano-sized mononuclear Cu (II) Schiff base complexes: design, characterization, molecular modeling and catalytic potentials in benzyl alcohol oxidation, Catal. Lett. 1146 (8) (2016) 1373–1396, doi:10.1007/s10562-016-1755-0.

[12] F. Nourifard, M. Payehghadr, Conductometric studies and application of new Schiff base ligand as carbon paste electrode modifier for mercury and cadmium determination, Int. J. Environ. Anal. Chem. 96 (6) (2016) 552–567 2, doi:10.1080/03067319.2016.1172219.

[13] L.P. Singh, J.M. Bhatnagar, Copper (II) selective electrochemical sensor based on Schiff Base complexes, Talanta 8 64 (2) (2020) 313–319, doi:10.1016/j.talanta.2004.02.020.

[14] W. Al Zoubi, N. Al Mohanna, Synthesis and antioxidant activities of Schiff bases and their complexes: a review: antioxidant activities of Schiff bases, Spectrochim. Acta A, Mol. Biomol. Spectrosc. 132 (2014) 854–870 11, doi:10.1002/aoc.3506.

[15] R.R. Pillai, K. Karrouchi, S. Fettach, S. Armaković, S.J. Armaković, Y. Brik, J. Taoufik, S. Radi, M.E. Faouzi, Synthesis, X-ray, spectroscopy, molecular docking and DFT calculations of (E)-N'-(2,4-dichlorobenzylidene)-5-phenyl-1H-pyrazole-3-carbohydrazide, J. Mol. Struct., 1177 5 (2019) 47–54, doi:10.1016/j.molstruc.2020.129714.

[16] P.H. Wang, J.G. Keck, E.J. Lien, M.M. Lai, Design, synthesis, testing, and quantitative structure-activity relationshipananlysis of substituted salicylaldehyde Schiff bases of 1-amino-3-hydroxyguanidine tosylate as new antiviral agents against coronavirus, J. Med. Chem. 33 (2) (1990) 608–614, doi:10.1021/jm00164a023.

[17] S.K. Bharti, G. Nath, R. Tilak, S.K. Singh, Synthesis, anti-bacterial and anti-fungal activities of some novel Schiff bases containing 2,4-disubstituted thiazole ring, Eur. J. Med. Chem. 45 (2) (2010) 651–660 1, doi:10.1016/j.ejmech.2009.11.008.

[18] S.A. Patil, C.T. Prabhakara, B.M. Halasangi, S.S. Toragalmath, P.S. Badami, DNA cleavage, antibacterial, antifungal and anthelmintic studies of Co(II), Ni(II) and Cu(II) complexes of coumarin Schiff bases: synthesis and spectral approach, Mol. Biomol. Spectrosc. 25 (2015) 137 641-51, doi:10.1016/j.saa.2014.08.028.

[19] S.E. Harpstrite, S.D. Collins, A. Oksman, D.E. Goldberg, V. Sharma, Synthesis, Characterization, and antimalerial activity of novel schiff-base-phenol and naphthalene-amine ligands, Med. Chem. (Shariqah (United Arab Emirates)) 4 (4) (2008) 392, doi:10.2174/157340608784872280.

[20] S. Murtaza, M.S. Akhtar, F. Kanwal, A. Abbas, S. Ashiq, S. Shamim, Synthesis and biological evaluation of schiff bases of 4-aminophenazone as an anti-inflammatory, analgesic, J. Saudi Chem. Soc. 21 (2017) S359–S372, doi:10.1016/j.jscs.2014.04.003.

[21] P.R. Nilkanth, S.K. Ghorai, A. Sathiyanarayanan, K. Dhawale, T. Ahamad, M.B. Gawande, S.N. Shelke, Synthesis and evaluation of anticonvulsant activity of some bases of 7-amino-1,3- dihydro-2H-1,4-benzodiazepin2-one, Chem. Biodivers. 17 (9) (2020) e2000342, doi:10.1002/cbdv.202000342.

[22] S.N. Mbugua, N.R. Sibuyi, L.W. Njenga, R.A. Odhiambo, S.O. Wandiga, M. Meyer, R.A. Lalancette, M.O. Onani, New Palladium (II) and Platinum (II) complexes based on pyrrole Schiff bases: synthesis, characterization, x-ray structure, and anticancer activity, ACS Omega 5 (25) (2020) 14942–14954, doi:10.1021/acsomega.0c00360.

[23] A.T. Shinde, N.J. Deshmukh, G.D. Kottapalle, S.B. Zangade, Syn. synthesis and antimicrobial evaluation of some new fluoro formazans, J. Pure Appl. Chem. Res. 5 (2) (2016) 61–66, doi:10.21776/ub.jpacr.2016.005.02.247.

[24] K. Govindarao, N. Srinivasan, R. Suresh, Synthesis, characterization and antimicrobial evaluation of novel Schiff bases of aryl amines based 2-azetidinones and 4-thiazolidinones, Res. J. Pharm. Tech. 13 (1) (2020) 168–172, doi:10.5958/0974-360X.2020.00034.7.

[25] É.N. Oiye, M.F.Muzetti M. Ribeiro, J.M. Toia Katayama, M.C. Tadini, M.A. Balbino, I.C. Eleotério, J. Magalhães, A.S. Castro, R.S. Mota Silva, J.W. da Cruz Júnior, E.R. Dockal, M.F. de, Oliveira electrochemical sensors containing Schiff bases and their transition metal complexes to detect analytes of forensic, pharmaceutical and environmental interest, Crit. Rev. Anal. Chem. 49 (2019) 488–509 6, doi:10.1080/10408347.2018.1561242.

[26] F.H. Al-Ostoot, S. Grisha, Y.H. Eissa Mohammed, H.K. Vivek, S.A. Khanum, Molecular docking synthesis of caffeic acid analogous and its anti-inflammatory, analgesic and ulcerogenic studies, Bioorg. Med. Chem. Lett. (2020) 127743, doi:10.1016/j.bmcl.2020.127743.

[27] F.H. Al-Ostoot, D.V. Geetha, Y.H. Eissa Mohammed, P. Akhileshwari, M.A. Sridhar, S.A. Khanum, Design-based synthesis, molecular docking analysis of an anti-inflammatory drug, and geometrical optimization and interaction energy studies of an indole acetamide derivative, J. Mol. Struct. 1202 (2020) 127244, doi:10.1016/j.molstruc.2019.127244.

[28] G. Sharma, S. Anthal, D.V. Geetha, F.H. Al-Ostoot, Y. Hussein Eissa Mohammed, S. Ara Khanum, M.A. Sridhar, R. Kant, Sythesis, structure and molecualr docking analysis of an anticancer drug of N-(2-aminophenyl)-2-(2-isopropylphenoxy) acatamide, Mol. Cryst. Liq. 675 (1) (2018) 85–95, doi:10.1080/15421406.2019.1624051.

[29] G.M. Sheldrick, Acta Cryst. A64 (2008) 112.

[30] A.L. Spek, PLATON, an integrated tool for the analysis of the results of a single crystal structure determination, Acta Cryst. A46 (1990) 34.

[31] C.F. Macrae, I.J. Bruno, J.A. Chisholm, P.R. Edgington, P. McCabe, E. Pidcock, L. Rodriguez-Monge, R. Taylor, J. van de Streek, P.A. Wood, J. Appl. Crysta. 41 (2) (2008) 466–470, doi:10.1107/S0021889807067908.

[32] D. Jayatilaka, S.K. Wolff, D.J. Grimwood, J.J. McKinnon, M.A. Spackman, Crystal-Explorer: a tool for displaying Hirshfeld surfaces and visualising intermolecular interactions in molecular crystals, Acta Crysta. A-found 62 (2006) S90 -S90.

[33] J.J. McKinnon, D. Jayatilaka, M.A. Spackman, Towards quantitative analysis of intermolecular interactions with Hirshfeld surfaces, Chem.Commun. (37) (2007) 3814–3816, doi:10.1039/B704980C.

[34] M.A. Spackman, J.J. McKinnon, Fingerprinting intermolecular interactions in molecular crystals, CrystEngComm 4 (66) (2002) 378–392, doi:10.1039/b203191b.

[35] M.A. Spackman, D. Jayatilaka, Hirshfeld surface analysis, CrystEngComm (11) (2009) 19–32, doi:10.1039/B818330A.

[36] C.F. Mackenzie, P.R. Spackman, D. Jayatilaka, M.A. Spackman, CrystalExplorer model energies and energy frameworks: extension to metal coordination compounds, organic salts, solvates and open-shell systems, IUCrJ 4 (2013) 575–587, doi:10.1107/S205225251700848X.

[37] M.J. Frisch, G.W. Trucks, H.B. Schlegel, G.E. Scuseria, M.A. Robb, J.R. Cheeseman, G. Scalmani, V. Barone, G.A. Petersson, H. Nakatsuji, X. Li, M. Caricato, A. Marenich, J. Bloino, B.G. Janesko, R. Gomperts, B. Mennucci, H.P. Hratchian, J.V. Ortiz, A.F. Izmaylov, J.L. Sonnenberg, D. Williams-Young, F. Ding, F. Lipparini, F. Egidi, J. Goings, B. Peng, A. Petrone, T. Henderson, D. Ranasinghe, V.G. Zakrzewski, J. Gao, N. Rega, G. Zheng, W. Liang, M. Hada, M. Ehara, K. Toyota, R. Fukuda, J. Hasegawa, M. Ishida, T. Nakajima, Y. Honda, O. Kitao, H. Nakai, T. Vreven, K. Throssell, J.A. Montgomery Jr., J.E. Peralta, F. Ogliaro, M. Bearpark, J.J. Heyd, E. Brothers, K.N. Kudin, V.N. Staroverov, T. Keith, R. Kobayashi, J. Normand, K. Raghavachari, A. Rendell, J.C. Burant, S.S. Iyengar, J. Tomasi, M. Cossi, J.M. Millam, M. Klene, C. Adamo, R. Cammi, J.W. Ochterski, R.L. Martin, K. Morokuma, O. Farkas, J.B. Foresman, D.J. Fox, Gaussian 09, Gaussian, Inc., Wallingford CT, 2016.

[38] R. Dennington, T. Keith, J. Millam, GaussView, Version 6.1.1, Semichem Inc., Shawnee Mission, KS, 2019.

[39] A. Bahrami, S. Seidi, T. Baheri, M. Aghamohammadi, A first- principles study on the absorption behavior of amphetamine on pristine, P-and Al-doprd B 12N 12 nano-cages, Superlattices Microstruct. (2013), doi:10.1016/j.spmi.2013.09.034.

[40] N.M. O'Boyle, A.L. Tenderholt, K.M. Langner, J. Comp. Chem. 29 (2008) 839–845.

[41] N.R. Bhavya, M. Mahendra, B.H. Doreswamy, Shamantha Kumar, Maryam Gilandoust, Nasseem Ahmad El-khatatneh Computational and spectroscopic investigations on boronic acid based fluorescent carbohydrate sensor in aqueous solution at physiological pH 7.5, J. Mol. Struct. 1194 (2019) 305–319, doi:10.1016/j.molstruc.2019.05.082.

[42] M. Alam, S. Park, Molecular structure, spectral studies, NBO, HOMO-LUMO profile, MEP and Mulliken analysis of 3β,6β-dichloro-5-hydroxy-5α–cholestane, J. Mol. Struct. 1159 (2018) 33–45, doi:10.1016/j.molstruc.2018.01.043.

[43] T. Lu, F. Chen, Multiwfn: a multifunctional wavefunction analyzer, J. comp. Chem. 33 (5) (2012) 580–592.

[44] S. Shukla, A. Srivastva, P. Kumar, P. Tandon, R. Maurya, R.B. Singh, Vibrational spectroscopic, NBO, AIM, and multiwfn study of tectorigenin: DFT approach, J. Mol. Struct. 1217 (2020) 128443, doi:10.1016/j.molstruc.2020.12844.

[45] W. Humphrey, A. Dalke, K. Schulten, VMD: visual molecular dynamics, J. mol. Graph. 14 (1) (1996) 33–38.